Electrochemical Self-Assembly of ZnO Nanoporous Structures

ARTICLE *in* THE JOURNAL OF PHYSICAL CHEMISTRY C · FEBRUARY 2007

Impact Factor: 4.77 · DOI: 10.1021/jp066447x

Electrochemical Self-Assembly of ZnO Nanoporous Structures

Gao-Ren Li,*,†,‡ Ci-Ren Dawa,† Qiong Bu,† Xi-Hong Lu,† Zhi-Hai Ke,† Hai-En Hong,† Fu-Lin Zheng,† Chen-Zhong Yao,† Guan-Kun Liu,† and Ye-Xiang Tong*,†

MOE of Key Laboratory of Bioinorganic and Synthetic Chemistry, School of Chemistry and Chemical Engineering, Institute of Optoelectronic and Functional Composite Materials, Sun Yat-Sen University, Guangzhou 510275, P. R. China, and State Key Lab of Rare Earth Materials Chemistry and Applications, Beijing 100871, P. R. China

Received: October 1, 2006; In Final Form: December 3, 2006

ZnO nanoporous structures were prepared on Cu substrates by electrochemical deposition in solutions of $ZnCl_2$ + ethylenediaminetetraacetic acid (EDTA) at a temperature of 90 °C. Cyclic voltammetry was used to study the electrochemical reactions relevant to the film growth. The transfer coefficient and diffusion coefficient of Zn(II) in 0.05 mol L^{-1} $ZnCl_2$ + 0.01 mol L^{-1} EDTA at 343 K were calculated as 0.276 and 5.12×10^{-10} m^2 s^{-1}, respectively. The synthetic parameters in this research allowed further structural manipulation for ZnO nanoporous films. The morphology evolvement from uniform planar foam structures to bricklike and spherelike foam structures could be realized by changing the current densities of electrodeposition. The PL spectra of the prepared ZnO samples show that few oxygen vacancies or interstitial Zn centers would be formed when the electrochemical deposition was carried out with a low current density ($\leq$0.1 mA/cm^2).

1. Introduction

Nanostructures and nanomaterials have attracted great interest with the help of the discovery of carbon nanotubes due to their novel fundamental properties and wide potential applications in many fields, and they are expected to play important roles in future technology. So far, various methods including chemical vapor deposition (CVD), template-assisted, vapor−liquid−solid (VLS), sol−gel, laser ablation, hydrothermal synthesis, and electrochemical deposition have been developed to prepare the nanostructures and nanomaterials.[1−8] Among all the preparation processes, electrochemical deposition has shown a powerful ability to control the crystallization engineering of the nanostructured thin films. Also, electrochemical deposition presents a simple, quick, and economical method for the preparation of large-area thin films, in terms of low-temperature processing, and arbitrary substrate shapes. The growth rate and film thickness can easily be well controlled by deposition potentials, current densities, and salt concentrations.

Zinc oxide (ZnO), one of the most attractive functional semiconductor materials for applications in photodetectors, photonic crystals, photodiodes, light-emitting diodes, gas sensors, varistors, and solar cells, is attracting more and more attention in both fundamental research and practical studies because of its specific optoelectronic and electrical properties as well as its excellent chemical and thermal stability.[9−14] It is well-known that the novel properties of nanostructured materials are obviously dependent on crystallinity, crystallite size, crystallographic orientation, and morphology. Therefore, development of a morphologically controllable synthesis of a ZnO semiconductor is urgently important to answer the demand for exploring the potential applications of ZnO.[15−20]

Most of the previous investigations in the electrochemical deposition of ZnO nanostructures mainly utilized $Zn(NO_3)_2$ as electrolyte.[21−24] However, $Zn(NO_3)_2$ potentially brings impurities, such as $Zn(OH)_2$ or $[Zn(OH)_4]^{2-}$, into the crystal lattices of ZnO during the electrodeposition of ZnO, and the impurities will be deleterious for the practical application of ZnO. Therefore, it seems necessary to investigate the relationship between electrodeposition conditions and morphologies of high-purity ZnO for exploring an effective and simple route to prepare novel ZnO nanostructures for practical applications. There are few reports on the preparation of ZnO by electrochemical deposition by using other Zn salts, such as $ZnCl_2$, as electrolytes despite the fact that the mechanism of the formation of ZnO in a solution of $ZnCl_2$ is obviously different from that in a solution of $Zn(NO_3)_2$. In this paper, we report that high-purity ZnO nanoporous structures have been formed directly onto copper substrates in a solution of $ZnCl_2$ by adding a complex reagent such as ethylenediaminetetraacetic acid [EDTA, $(CH_2N)_2(CH_2COOH)_4$] as a shape-control reagent. The solution of $ZnCl_2$ is found to be an appropriate and cheap deposition medium for the formation of high-purity ZnO nanoporous structures with the help of EDTA. The prepared high-density ZnO nanoporous structures are very promising candidates for hydrogen storage because their active surface area is much larger than that of nanowire structures.[25−26]

2. Experimental Section

A simple three-electrode cell was used in our experiments. The working electrode used in the cyclic voltammogram (CV) was Pt (99.99%, 0.1 cm^2). In electrochemical deposition, a graphite rod with a surface area of 4.0 cm^2 was used as the auxiliary electrode, a saturated calomel electrode (SCE) was used as the reference electrode that was connected to the cell with a double salt bridge system, and pure copper foil was used as the working electrode. The electrochemical deposition of the thin films of ZnO was carried out in $ZnCl_2$ aqueous solutions. In order to control the surface shapes of ZnO films, EDTA was added to the deposition baths. The electrochemical depositions were carried out on Cu substrates under galvanostatic conditions

* Corresponding authors. E-mail: ligaoren@mail.sysu.edu.cn (Gao-Ren Li); chedhx@mail.sysu.edu.cn (Ye-Xiang Tong).

† Sun Yat-Sen University.

‡ State Key Lab of Rare Earth Materials Chemistry and Applications.

10.1021/jp066447x CCC: $37.00
Published on Web 01/18/2007

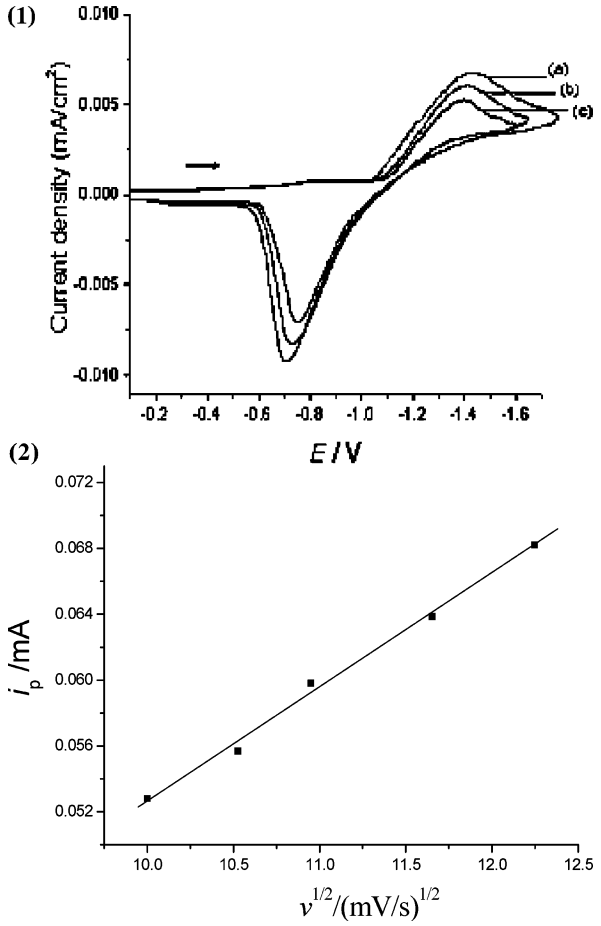

Figure 1. (1) Cyclic voltammograms of Pt electrodes in 0.05 mol L^{-1} $ZnCl_2$ + 0.01 M EDTA at 343 K at different sweep rates: (a) 150 mV/s, (b) 120 mV/s, (c) 100 mV/s. (2) The plot of i_p versus $v^{1/2}$ according to the cyclic voltammograms in (1).

with current densities between 1 and 0.01 mA/cm^2. The Cu substrate was cleaned ultrasonically in 0.1 M HCl, distilled water, and acetone and then rinsed in distilled water again. All the electrochemical deposition experiments were carried out in a configured glass cell at 70−90 °C. The cyclic voltammetry and electrochemical deposition experiments were done with a Chi750 electrochemical workstation. The deposits were characterized by energy-dispersive spectroscopy (EDS), X-ray diffraction (XRD), and field emission−scanning electron microscope (FE-SEM), respectively. The photoluminescence (PL) measurements were carried out on a fluorescence spectrophotometer at room temperature, and the excited wavelength was 325 nm.

3. Results and Discussion

Figure 1(1) shows the cyclic voltammogram of the Pt electrode in 0.05 mol L^{-1} $ZnCl_2$ + 0.01 M EDTA at 343 K at different sweep rates. From these curves, we can observe that one cathodic peak appeared. These cathodic waves corresponded to the reduction of Zn(II), namely, Zn(II) + 2e → Zn. The cathodic peak potentials (E_p) shifted negatively with the increasing of sweep rates (v) as shown in Figure 1(1). Also, the cathodic peak current (i_p) linearly increased with the increase of $v^{1/2}$ (Figure 1(2)). All these characteristics indicated that the reduction of Zn(II) was irreversible. From Figure 1(1), we could obtain that the half peak potential ($E_{P/2}$), the peak potential (E_P), and $|E_{P/2} - E_p| = 0.10$ V, and the $\alpha = 0.276$ can be obtained as the electron-transfer number n is 2.0. At 298 K, the

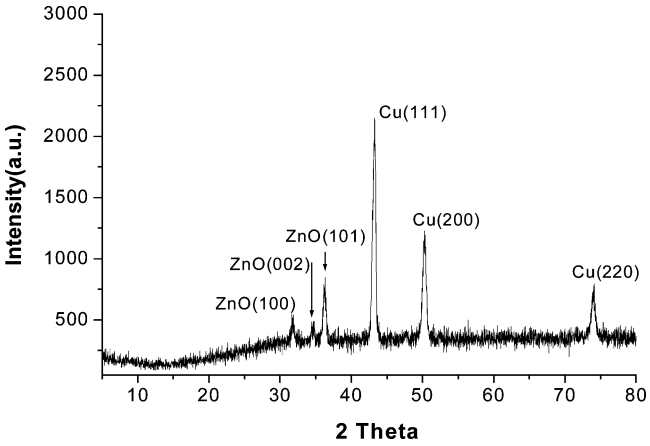

Figure 2. XRD patterns of the synthesized ZnO nanoporous structures prepared in 0.05 mol L^{-1} $ZnCl_2$ + 0.01 M EDTA at 343 K with a current density of 0.05 mA/cm^2.

relationship between peak current (i_p) and potential sweep rate (v) is $i_p = (2.99 \times 10^5)n^{3/2}\alpha^{1/2}Ac_o{}^*D^{1/2}v^{1/2}$ (where i_p, A, and D stand for peak current, electrode area, and diffusion coefficient, respectively); $D = 5.12 \times 10^{-10}$ m^2 s^{-1} can be calculated from the plot of i_p versus $v^{1/2}$ for the reduction peak shown in Figure 1(2).

Galvanostatic electrolysis was carried out in solutions of the mixture of $ZnCl_2$ and EDTA. During the electrochemical deposition of ZnO, the substances on Cu substrates are known to be obviously affected by the temperatures and current densities of deposition. Higher temperatures promote the corrosion of the electrodeposited Zn to form the stable passive-phase ZnO via chemical reaction (eqs 1 and 2):[23,24]

$$Zn(s) + H_2O(l) = ZnO(s) + H_2(g) \quad (1)$$

$$2Zn(s) + O_2(g) \rightarrow 2ZnO(s) \quad (2)$$

which are thermodynamically spontaneous under the conditions of our experiments. (Some oxygen in the air was dissolved in deposition solution.) Here, there is a competitive reaction of the electrodeposition of Zn and the corrosion of electrodeposited Zn. When the electrochemical deposition rate is slower than the corrosion rate, all of the deposited Zn can be converted to ZnO successfully. At a high current density (>10.00 mA/cm^2) and a low temperature (<15 °C), the electrochemical deposition rate is faster than the corrosion rate, and thus a mixture of Zn and ZnO phases will be obtained. The substances on Cu substrates will be mostly ZnO when the electrochemical deposition is carried out at a high deposition temperature (>90 °C) and a low current density (1.00 mA/cm^2). Here we could successfully get high-purity ZnO films on the Cu substrate when the electrochemical deposition was carried out in $ZnCl_2$ solution under the conditions of 90 °C and 0.05 mA/cm^2.

Figure 2 shows the XRD patterns of the electrodeposited ZnO films with nanoporous structures. All of the XRD patterns of ZnO can be indexed as hexagonal wurtzite structures (hexagonal phase, space group *P*63*mc*) according to JCPDS card (No. 36-1451). The surface morphologies of the ZnO films electrodeposited with a current density of 0.05 mA/cm^2 were examined with scanning electron microscopy (SEM, JEOL JSM-6330F), and the typical SEM images of ZnO films are shown in Figure 3 at different magnifications. As shown in Figure 3a, it can be observed that the surface is composed of numerous nanosized pores which lead to high superficial volume and low mass

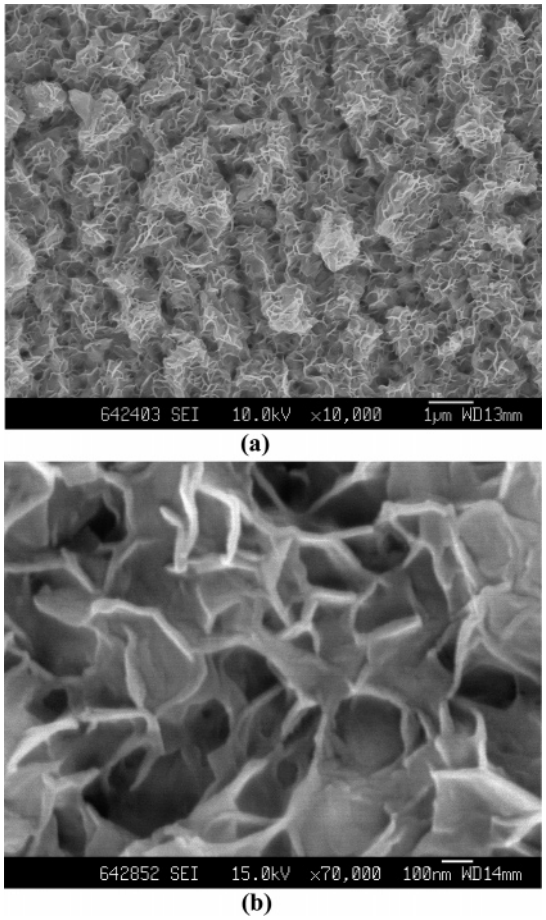

Figure 3. SEM images of the ZnO nanoporous structures fabricated via electrochemical deposition in solutions of 0.05 M $ZnCl_2$ + 0.01 M EDTA with a current density of 0.05 mA/cm^2 at different magnifications: (a) 10000×, (b) 70000×.

density. Also, it contains an extensive growth of sheetlike structures. To further examine the surface structure of these porous ZnO structures, a high-magnification SEM image was obtained and is shown in Figure 3b. The porous structures were actually composed of a random growth of seemingly flexible nanosheets that can be bent and connected with each other. The thicknesses of these nanosheets mostly range between 10 and 20 nm. However, the nonporous ZnO films were obtained when the electrodeposition was carried out in the absence of EDTA (see Supporting Information, Figure S1). The mechanism for the formation of nanoporous structures of ZnO is still under investigation. The strong chelation between Zn^{2+} and EDTA must be a reason for the formation of nanoporous structures. In the presence of EDTA, the EDTA will chelate strongly with Zn^{2+}, which will dramatically decrease the concentration of free Zn^{2+} in the solution. Thus, the electroreduction of Zn^{2+} is relatively slow, and the newly deposited Zn has enough time to react with H_2O or the carboxyl in EDTA before the aggregation of the later-deposited Zn. The formed nanoporous structures can be explained as the result of hydrogen bubbles functioning as a dynamic template during metal deposition. Since the oxidation−reduction potential of the Zn element is very negative and the element is very active, the electrodeposited Zn could create a large number of hydrogen bubbles with H_2O or the carboxyl in EDTA on the copper substrate that will move toward the electrolyte/air interface during the electrodeposition process. Thus, the metal growth toward the gas bubble is prohibited simply because there are no metal ions available there, leading to deposition only between gas bubbles and

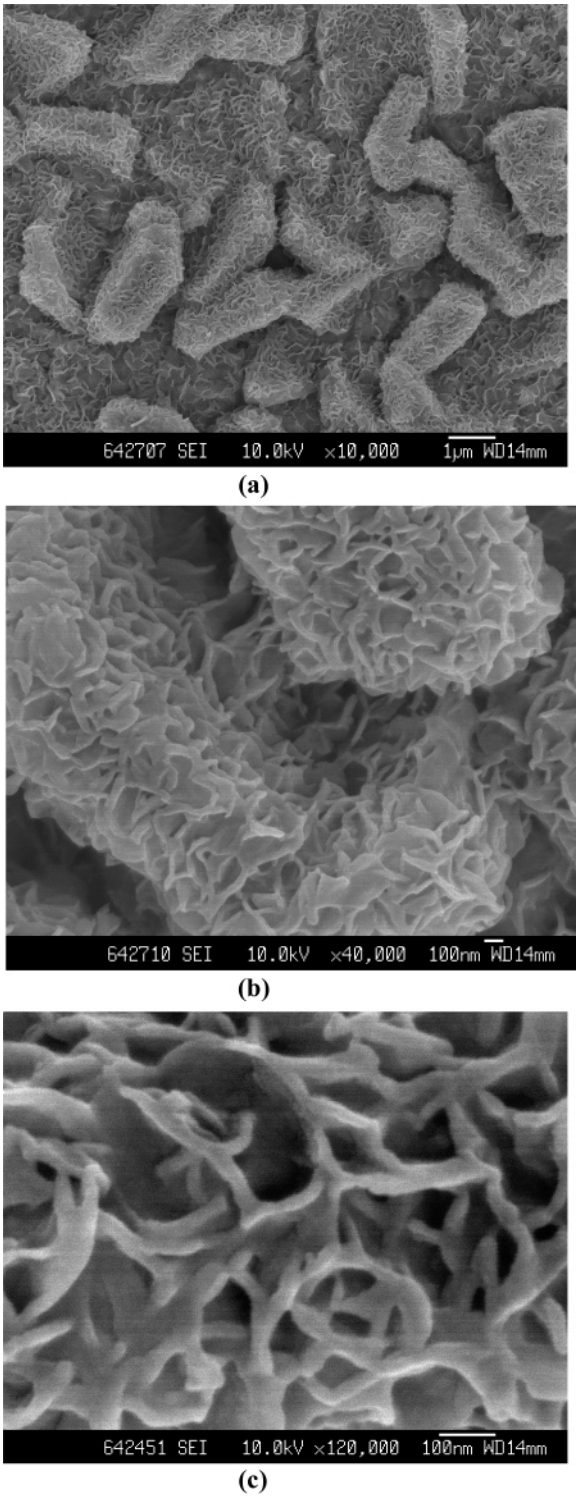

Figure 4. SEM images of the ZnO nanoporous bricklike particles fabricated via electrochemical deposition in solutions of 0.05 M $ZnCl_2$ + 0.01 M EDTA with a current density of 0.1 mA/cm^2 at different magnifications: (a) 10000×, (b) 40000×, (c) 120000×.

formation of nanosized pores. The porous structure is caused by the competitive reaction of the electrodeposition and hydrogen evolution. The formation of sheetlike nanostructures is also believed to result from the actions of Cl^- and EDTA. There are two polar surfaces and six side facets in the hexagonal wurtzite ZnO, and they are generally bound by the (0001) and (100) families of planes, respectively.[27−29] It has been demonstrated that adsorption of Cl^- takes place preferentially onto the (0001) plane of ZnO, and it is favored to produce plateletlike

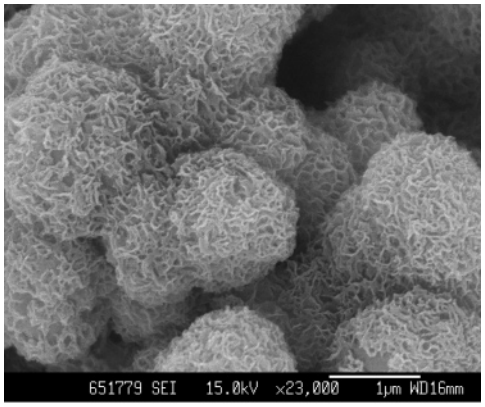

(a)

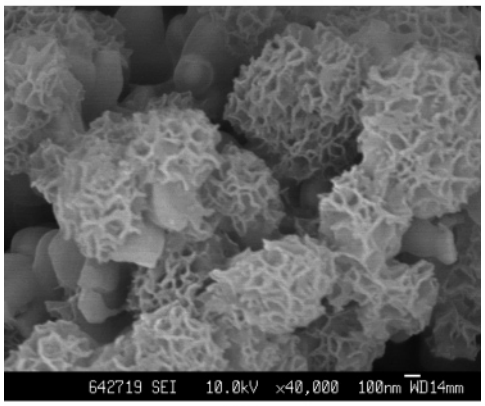

(b)

Figure 5. SEM images of the ZnO nanoporous particles fabricated via electrochemical deposition in solutions of 0.05 M $ZnCl_2$ + 0.01 M EDTA with a current density of (a) 0.5 mA/cm^2, (b) 1 mA/cm^2.

or sheetlike crystals.[29] In the presence of EDTA, which may also preferentially adsorb to certain surfaces of the ZnO nucleation seeds and alter the crystal growth process, an extensive growth of flexible nanosheets results. With the nanosheets clustered together during the growth process through the interconnection of the nanosheets and the hydrogen bubbles moving, the porous ZnO with sheetlike nanostructures are eventually formed.

When the current density of electrodeposition was increased to 0.10 mA/cm^2, many nanoporous bricklike particles were obtained as shown in Figure 4a and b. It can be more clearly seen that the surfaces are composed of numerous nanosized pores as shown in Figure 4c which has a larger magnification (120000×), and the pores are more uniform than those in Figure 3. At the same time, we can observe that the area around the pores was also composed of plentiful and out-of-order sheetlike nanostructures, and the thickness was about 10−20 nm. However, the nanoporous spherical structures could be obtained when the deposition current was further increased to 0.50 mA/cm^2 as shown in Figure 5a. The morphology evolvement from uniform planar foam structures to bricklike and spherelike foam structures can be explained as follows. With the increase of the current density of deposition, the larger current density will result in the faster release of Zn^{2+}, and a larger quantity of nucleates will be produced. These deposited nucleates will aggregate together and adopt an appropriate structure in order to keep their surface energy low. It is believed that the reduction in surface energy is the primary driving force for simple particle growth, and the further reduction in surface energy due to the

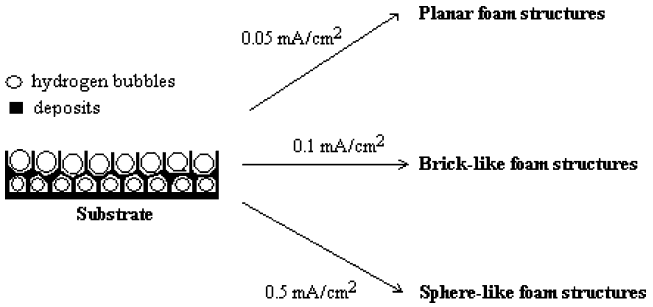

Figure 6. A schematic illustration for the formation mechanism of various ZnO foams.

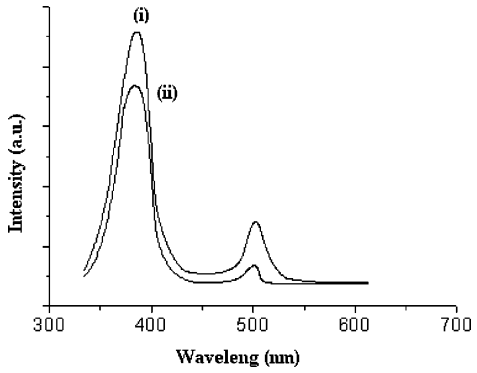

Figure 7. PL spectra of the ZnO nanoporous particles fabricated via electrochemical deposition in the solution of 0.05 M $ZnCl_2$ + 0.01 M EDTA with a current density of (i) 0.1 mA/, (ii) 0.5 mA/cm^2.

minimization of high-surface-energy faces will drive the morphology evolution.[30] Therefore, the surface morphology finally evolved to the spherelike foam structures, which have the lowest surface energy, when the current density was increased to 0.50 mA/cm^2. However, when the current density of deposition was further increased to 1.0 mA/cm^2, some defects were formed because of the fast growth of nucleates, which produced some nanocrystals that are nonporous as shown in Figure 5b. As the nucleate was produced very fast, some formed nucleate almost had no time to react with H_2O or the carboxyl in EDTA before it was buried by the later deposits. Therefore, the obtained products were composed of the nanoporous spherical structures and some nonporous nanocrystals, and the composition of the obtained products was a mixture of Zn and ZnO. The XRD and EDS of the above samples are provided in Supporting Information (Figures S2 and S3) to support this conclusion. A schematic illustration for the formation mechanism of various ZnO foam structures is shown in Figure 6 and gives general readers a clear understanding of this formation process.

The PL properties of the different ZnO nanoporous structures were investigated, and the room-temperature PL spectra are shown in Figure 7. The dominant peaks at about 384 nm are observed, and it can be attributed to free-exction. A weak deep level emission at 500 nm related to oxygen vacancy or interstitial zinc in Figure 7(i) is almost negligible, which indicates that these ZnO electrodeposits are highly crystallized and of excellent optical quality. The PL spectra of ZnO samples shown in Figure 7 reveal that the intensity of the green emission increased with the addition of the current density of the electrodeposition. When the electrochemical deposition was carried out with the higher current density, the electroreduction rate of Zn^{2+} was higher and leads to the faster formation of ZnO samples, and more oxygen vacancies or interstitial Zn centers will be formed. These defect centers acted as the origin of the green emission.

4. Conclusions

ZnO nanoporous structures can be fabricated in solutions of $ZnCl_2$ despite the fact that the electrodeposition was not carried out in the solution of $Zn(NO_3)_2$ that is used widely by most researchers. The morphology evolvement from uniform planar foam structures to bricklike and spherelike foam structures can be realized when the electrodeposition of ZnO was carried out in the solution of the mixture of $ZnCl_2$ and EDTA at 90 °C with different current densities. The PL spectra of the prepared ZnO samples show that few oxygen vacancies or interstitial Zn centers will be formed when the electrochemical deposition was carried out with a low current density. Using $ZnCl_2$ solutions with appropriate capping agents is a simple and efficient path to prepare the different ZnO nanostructures via the electrochemical method, and this approach can be expected to provide a versatile and facile pathway for designing ZnO nanoporous structures with novel morphologies. The unique synthetic mechanism of this approach is also expected to be widely used in the investigation of the electrodeposition of other metallic and semiconducting nanostructures and nanomaterials.

Acknowledgment. We appreciate this work was supported by the Natural Science Foundations of China (Grant No. 20603048 and 20573136), the Natural Science Foundations of Guangdong Province (Grant No. 06300070, 06023099, and 04205405), and the Foundations of Potentially Important Natural Science Research and Young Teacher Starting-up Research of Sun Yat-Sen University.

Note Added after ASAP Publication. This paper was published ASAP on January 18, 2007. Units were added to Figure 1 (2) labels, and the spelling of an author's name was corrected. The updated paper was reposted on January 24, 2007.

Supporting Information Available: SEM image of a ZnO film electrodeposited without EDTA (Figure S1). EDS (Figure S2) and XRD (Figure S3) of the samples electrodeposited with a current density of 1.0 mA/cm^2. This material is available free of charge via the Internet at http://pubs.acs.org.

References and Notes

(1) Kaul, A. B.; Wong, E. W.; Epp, L.; Hunt, B. D. *Nano Lett.* **2006**, *6*, 942−947.

(2) Lu, Q.; Gao, F.; Komarneni, S.; Mallouk, T. E. *J. Am. Chem. Soc.* **2004**, *126*, 8650−8651.

(3) Ma, C.; Wang, Z. L. *Adv. Mater.* **2005**, *17*, 2635−2639.

(4) Célérier, S.; Laberty-Robert, C.; Long, J. W.; Pettigrew, K. A.; Stroud, R. M.; Rolison, D. R.; Ansart, F.; Stevens, P. *Adv. Mater.* **2006**, *18*, 615−618.

(5) Sylvestre, J.-P.; Kabashin, A. V.; Sacher, E.; Meunier, M.; Luong, J. H. T. *J. Am. Chem. Soc.* **2004**, *126*, 7176 −7177.

(6) Tomita, K.; Petrykin, V.; Kobayashi, M.; Shiro, M.; Yoshimura, M.; Kakihana, M. *Angew. Chem., Int. Ed.* **2006**, *45*, 2378−2381.

(7) Gole, J. L.; Prokes, S. M.; Stout, J. D.; Glembocki, O. J.; Yang, R. *Adv. Mater*. **2006**, *18*, 664−667.

(8) Endres, F.; Bukowski, M.; Hempelmann, R.; Natter, H. *Angew. Chem., Int. Ed.* **2003**, *42*, 3428−3430.

(9) (a) Gao, P. X.; Wang, Z. L. *J. Am. Chem. Soc.* **2003**, *125*, 11299. (b) Wang, Z. L.; Song, J. H. *Science* **2006**, *312*, 242.

(10) Choi, K.-S.; Lichtenegger, H. C.; Stucky, G. D.; McFariand, E. W. *J. Am. Chem. Soc.* **2002**, *124*, 12402.

(11) Zhang, J.; Sun, L.; Yin, J.; Su, H.; Liao, C.; Yan, C. *Chem. Mater*. **2002**, *14*, 4172.

(12) Wang, X. D.; Summers, C. J.; Wang, Z. L. *Nano Lett.* **2004**, *4*, 423.

(13) Lao, J. Y.; Wen, J. G.; Ren, Z. F. *Nano Lett.* **2002**, *2*, 1287.

(14) Hu, J. Q.; Bando, Y.; Zhan, J. H.; Li, Y. B.; Sekiguchi, T. *Appl. Phys. Lett.* **2003**, *83*, 4414.

(15) Park, W. I.; Yi, G.-C.; Kim, M.; Pennycook, S. J. *Adv. Mater.* **2002**, *14*, 1841−1843.

(16) Mo, M.; Yu, J. C.; Zhang, L. Z.; Li, S.-K. A. *Adv. Mater.* **2005**, *17*, 756−760.

(17) Wu, J.-J.; Liu, S.-C. *Adv. Mater*. **2002**, *14*, 215−218.

(18) Li, F.; Ding, Y.; Gao, P.; Xin, X.; Wang, Z. L. *Angew. Chem., Int. Ed.* **2004**, *43*, 5238−5242.

(19) Pacholski, C.; Kornowski, A.; Weller, H. *Angew. Chem., Int. Ed.* **2004**, *43*, 4774−4777.

(20) Greene, L. E.; Law, M.; Goldberger, J.; Kim, F.; Johnson, J. C.; Zhang, Y.; Saykally, R. J.; Yang, P. *Angew. Chem., Int. Ed.* **2003**, *42*, 3031−3034.

(21) Yoshida, T.; Terada, K.; Schlettwein, D.; Oekermann, T.; Sugiura, T.; Minoura, H. *Adv. Mater*. **2000**, *12*, 1214−1217.

(22) Choi, K. S; Lichtenegger, H. C.; Stucky, G. D.; McFarland, E. W. *J. Am. Chem. Soc.* **2002**, *124*, 12402−12403.

(23) Pauporte, T.; Yoshida, T.; Cortes, R.; Froment, M.; Lincot, D. *J. Phys. Chem. B* **2003**, *107*, 10077−10082.

(24) Tan, Y.; Steinmiller, E. M. P.; Choi, K. S. *Langmuir* **2005**, *21*, 9618−9624.

(25) Kim, S.-W.; Fujita, S.; Yi, M.-S.; Yoon, D. H. *Appl. Phys. Lett.* **2006**, *88*, 253114.

(26) Wan, Q.; Lin, C. L.; Yu, X. B.; Wang, T. H. *Appl. Phys. Lett.* **2004**, *84*, 124.

(27) Vanheusden, K.; Warren, W. L.; Seager, C. H.; Tallant, D. R.; Voigt, J. A.; Gnade, B. E. *J. Appl. Phys.* **1996**, *79*, 7983.

(28) Li, Y.; Cheng, G. S.; Zhang, L. D. *J. Mater. Res.* **2000**, *15*, 2305.

(29) Xu, L.; Guo, Y.; Liao, Q.; Zhang, J.; Xu, D. *J. Phys. Chem. B* **2005**, *109*, 13519−13522.

(30) Xu, H.; Wang, W.; Zhu, W. *J. Phys. Chem. B* **2006**, *110*, 13829−13834.